




RESEARCH ARTICLE

Process Systems Engineering

Process modeling guides operational variables that affect CO₂ utilization during the accelerated carbonation of concrete

Dale P. Prentice^{1,2}  | Othman AlShareedah^{1,2} | Manas Sarkar^{1,2} |
 Jenny Arabit^{1,2} | Iman Mehdipour³ | Shaik Afzal⁴ | Junwei Luo⁵ |
 Fahim Abdullah⁵ | Sungil Yun⁵ | Panagiotis D. Christofides⁵  |
 Dante Simonetti^{2,5}  | Gaurav Sant^{1,2,6,7}

¹Laboratory for the Chemistry of Construction Materials (LC²), Department of Civil and Environmental Engineering, University of California, Los Angeles, California, USA

²Institute for Carbon Management (ICM), University of California, Los Angeles, California, USA

³CarbonBuilt Inc., Los Angeles, California, USA

⁴GTI Energy, Des Plaines, Illinois, USA

⁵Department of Chemical and Biomolecular Engineering, University of California, Los Angeles, California, USA

⁶Department of Materials Science and Engineering, University of California, Los Angeles, California, USA

⁷California Nanosystems Institute (CNSI), University of California, Los Angeles, California, USA

Correspondence

Panagiotis D. Christofides and Dante Simonetti, Department of Chemical and Biomolecular Engineering, University of California, Los Angeles, CA 90095, USA.
 Email: pdc@seas.ucla.edu and dasimonetti@ucla.edu

Gaurav Sant, Laboratory for the Chemistry of Construction Materials (LC²), Department of Civil and Environmental Engineering, University of California, Los Angeles, CA 90095, USA.
 Email: gsant@ucla.edu

Funding information

University of California's Office of the President via the Carbon Neutrality Initiative; Pritzker Chair in Sustainability; National Energy Technology Laboratory, Grant/Award Number: DE-FE0031915

Abstract

Accelerated concrete carbonation is an expanding option for decarbonizing construction. Factors such as concrete mixture design and carbonation environment can influence the maximum CO₂ utilization that can be achieved during such a process. A carbonation process designed to utilize a water-saturated dilute CO₂ source wherein $2 < \text{CO}_2 \text{ concentration (v/v\%)} < 16$, was modeled in AspenPlus®. A regression model was developed to correlate CO₂ uptake, relative humidity (11%–100%), CO₂ concentration ($[\text{CO}_2] = 2\text{--}16 \text{ v/v\%}$), and temperature ($T = 11\text{--}74^\circ\text{C}$) conditions within a carbonation reactor. It was determined that $[\text{CO}_2]$ was the most significant variable as higher concentrations enhanced CO₂ transport through the concrete. The energy use intensity per mass of CO₂ utilized (kWh/kgCO₂) was determined across a range of processing conditions. As a function of the operational conditions, accelerated carbonation provides a net CO₂ reduction of up to 28 kgCO₂/tonne of concrete; a reduction of up to ~45% compared to typical formulations.

KEYWORDS

carbonation, CO₂ utilization, concrete, decarbonization, process modeling

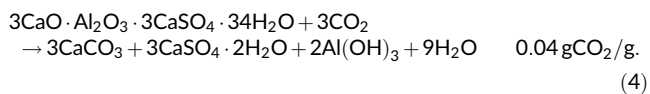
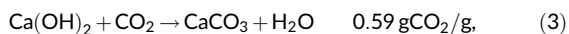
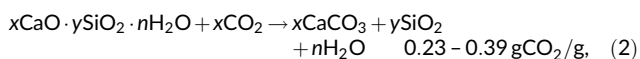
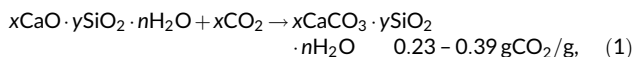
1 | INTRODUCTION AND BACKGROUND

Anthropogenic sources of carbon dioxide are generated from several sources including the combustion of fossil fuels, and the production of Ordinary Portland Cement (OPC).¹ Cement production results in CO₂

release associated with the thermal decomposition of its mineral carbonate feedstocks.¹ In combination, limestone's decomposition and the thermal requirements of the clinkering process cause OPC production to contribute ~10% of annual global CO₂ emissions.^{1–5} To reduce the CO₂ footprint of concrete production, a CO₂

mineralization technology that utilizes flue gas, biomass, or direct air capture derived CO₂ has been developed. This approach involves the replacement of OPC in concrete by less CO₂-intensive materials (e.g., fly ashes) and materials that feature a capacity for significant CO₂ uptake (e.g., portlandite), making them amenable for use in accelerated carbonation solutions.

Concrete consists of 10–20 mass % OPC depending on its end-use application.^{6–10} Depending on their composition, different compounds endemic to OPC-based systems feature different levels of CO₂ uptake^{2,11} as shown in Equations (1)–(4), ranging from 0.04 to 0.6 g CO₂/g solid.



As shown in Equation (3), portlandite (Ca(OH)₂) features a substantial capacity for CO₂ uptake, and in fact the carbonation of this material has been shown to enhance strength by reducing the porosity of the concrete mixture by converting the Ca(OH)₂ to CaCO₃ that is associated with an increase in the molar volume of the product (CaCO₃) vis-à-vis, the reactant (Ca(OH)₂).^{6,12} While OPC-based concrete does indeed have the potential to carbonate naturally, accelerated carbonation approaches are far more effective on account of its ability to overcome the diffusive/transport-limitations that hinder the natural carbonation of concrete. In this vein, recent studies have shown that accelerated concrete carbonation is feasible across a range of CO₂ concentrations, temperatures, and relative humidity (RH; 5 < [CO₂] < 100 v/v%, 10 < T < 90°C, and 10 < RH < 100%).^{7,12–15} Unsurprisingly, while elevated temperatures improve CO₂ transport (diffusion), the solubility of aqueous CO₂ decreases with temperature. However, the higher temperatures increase the drying rate of concrete, thus reducing the pore saturation and promoting greater CO₂ diffusivity.^{14,16} For these reasons, a careful balance of parameters including the carbonation duration, temperature, RH, and the CO₂ concentration are necessary to maximize CO₂ uptake.

Accelerated carbonation durations can range from 2 h to 56 days. The longer timespans past 24 h are likely impractical from a commercial perspective.^{7,12,15} Carbonation curing can be carried out within pressure vessels or ambient-pressure flow-through reactors. Flow-through reactors are generally far less energy-intensive.^{13,17} Gaseous CO₂,^{7,12–15} as opposed to supercritical CO₂, is generally adopted for these applications as it is considered more practical and widely accessible.¹⁸ Of the studies considering gaseous CO₂, most studies consider

pure CO₂ streams which are generally uneconomical, in spite of the enormous amount of CO₂ that is available from natural gas combustion, coal combustion, biomass production, and cement plant flue gas streams (ranging from 4 to 40 vol.%), albeit at lower concentrations.¹⁹

Although many carbonation models are available for determining the CO₂ uptake of concrete, few if any studies have modeled the larger-scale accelerated carbonation process and the extent of CO₂ reduction that may be achievable.^{13,14,16,20} Towards this end, a concrete carbonation process utilizing a flow through reactor operating at near ambient conditions is modeled.²¹ The process considers a static CO₂-rich source, for example, biomass-derived flue gas with the following conditions: 2% < CO₂ < 16% vol.%, 11 < T < 74°C, and fully saturated moisture conditions.^{22–27} An AspenPlus© model was developed that incorporates regressed relationships for a representative concrete formulation and geometry that allows estimation of the CO₂ uptake as a function of the [CO₂], temperature, and RH, as measured at the bench-scale. The purpose of this modeling approach is to provide guidance for larger-scale concrete producers to expand this concrete production process from the bench-scale to large-scale production.

2 | MATERIALS AND METHODS

2.1 | Regression model development

2.1.1 | Mixing and sample fabrication

Dry-cast concrete was mixed at a low water-to-binder mass ratio ($w/b = 0.29$, i.e., having zero slump) and then consolidated by mechanical compaction to achieve the desired shape (i.e., with a surface-to-volume ratio [s/v , per mm] of 0.08 per mm, to represent a Concrete Masonry Unit: CMU). The concrete formulation used consisted of 10 mass % Type III OPC, 5 mass % portlandite (93 mass % purity, as measured by thermogravimetric analysis), 5 mass % Class C fly ash, and fine and coarse aggregates (22 mass % coarse with a size ranging between 1.18 and 4.75 mm, and 58 mass % fine river sand compliant with ASTM C33²⁸). The concrete was used to fabricate a cylindrical sample (76 mm: diameter, 76 mm: height) by placement in a metallic mold. Thereafter, the material was compacted by applying 15 MPa of compaction stress at a loading rate of 0.9 kN/s followed by a stress hold for 15 s after which the compaction stress was released. Thereafter, the compacted concrete sample was removed from the mold and subjected to accelerated carbonation curing.

2.1.2 | Carbonation curing

Concentrated CO₂ (purity >99.5 vol.%) and compressed air were mixed using mass flow controllers (Alicat) to achieve a specific CO₂ concentration following which the gas stream was input into the bench-scale carbonation reactor (Figure 1). The temperature, RH, and

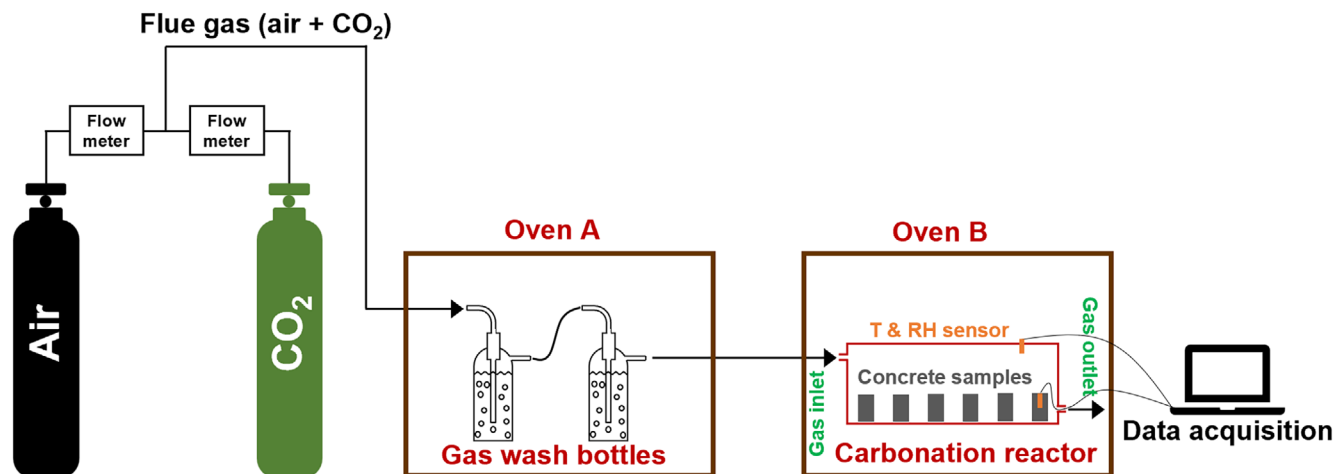


FIGURE 1 A schematic of the CO₂ mineralization process. The CO₂-containing stream is humidified using the gas wash bottles and streamed into the flow-through carbonation reactor. The *T*, relative humidity (RH) and CO₂ concentration within the reactor are monitored in real-time using computer-linked sensors.

CO₂ concentration in the reactor were measured continuously using Dracal USB-DXC220 sensors. The RH was controlled by bubbling the gas through two wash bottles placed in series in a convective oven (Quincy Lab Inc.). The temperature of Oven A was adjusted to achieve the desired gas RH, and Oven B was used to control the target temperature within the reactor.

2.1.3 | Material characterization

To quantify the extent of carbonation, a hand-held rotary drill was used to extract powder samples up to its mid-depth (38 mm). Thereafter, the extracted powder was collected and immersed in isopropyl alcohol (IPA) and continuously stirred for 24 h to arrest OPC hydration. The powder was then collected using vacuum filtration, dried in a desiccator, and analyzed using thermogravimetric analysis (TGA). TGA was carried out using an STA 6000 (Perkin Elmer). A temperature range of 35–950°C and a heating rate of 15°C/min were used in the presence of ultrahigh purity N₂ gas (purity >99.99%) at a flow rate of 20 mL/min. The CO₂ content (mass % of total solids) of the sample was quantified using the following equation to calculate the difference in the residual mass at a temperature range between 600 and 900°C at which mineral carbonates (such as CaCO₃) decompose^{29,30}:

$$m_{\text{CO}_2} = \frac{m_{(600-900^\circ\text{C})}}{m_{\text{solid}}} \times 100, \quad (5)$$

where m_{CO_2} is the mass percentage of CO₂ determined from TGA (mass %), $m_{(600-900^\circ\text{C})}$ is the mass loss between 600 and 900°C (mg), and m_{solid} is the mass of the solid sample (mg). The initial content of CO₂ in the pre-carbonated samples was subtracted from the post-carbonation assessment to account for CO₂ that was specifically taken up during the carbonation process.

2.1.4 | Regression model development

A parametric approach was followed to assess the influence of processing conditions on the CO₂ uptake of a dry-cast concrete component. Design-Expert 7, which applies a Design-of-Experiments method, was used to generate the experimental matrix and model the results using a response surface methodology.³¹ Central composite design (CCD) was used with minimal point designs to limit the required experiments to generate the regression model. In the CCD method, the center point (i.e., 0) represents the middle value of each parameter. For the factorial points, each variable was changed to the upper limit or the lower limit. The distance from the center point to the upper and lower limits of each variable was multiplied by α , a factor used to determine the distance from the center point to the axial points. The experimental matrix for different processing conditions is shown in Table S2 (see Supplementary Information Section S1).

An analysis of variance (ANOVA) approach was used to assess the significance of the model parameters using least-squares fitting. A temperature range of 11–74°C was selected.³² The RH of the reactor ranged between 11% and 100% while the CO₂ concentration ranged between 2 and 16 v/v%; that is, a range that encompasses CO₂ emission concentrations emitted by natural gas, coal fired, and biomass power plants. The extent of carbonation of the concrete was presented as the conversion level (*X*, unitless), which represents the ratio of the CO₂ uptake at any time to the maximum (stoichiometric) CO₂ uptake. For example, the maximum (stoichiometric) CO₂ uptake of portlandite is 0.59 gCO₂/g_{CH}.^{22,33} On the other hand, the maximum CO₂ uptake of OPC was estimated as 0.19 gCO₂/g_{solid} (see Supplementary Information Section S2). The CO₂ uptake of the fly ash was calculated as 0.02 gCO₂/g_{FA} for carbonation occurring at 80% RH and 65°C in a pure (100 vol.%) CO₂ atmosphere after 24 h of carbonation of the particulates. Based on the carbonation data of the components, the maximum CO₂ uptake of the ternary formulation was assessed as 0.045 gCO₂/g_{solid}.

2.2 | Heat and mass transfer modeling using AspenPlus©

An integrated concrete masonry production-CO₂ utilization (carbonation) process was modeled at a pilot scale (i.e., 10,000 kg of CMU production per day). The process model was developed using AspenPlus© ver. 12.1. eNRTL was selected as the thermodynamic property package for the vapor-liquid phase.³⁴ This method explicitly accounts for the gas- and liquid-phase chemistry and considers the specific heat capacities of H₂O, CO₂, and N₂ in the analysis. The following APV732 property databanks were used: ASPENPCD, AQUEOUS, SOLIDS, INORGANIC, and PURGE26. The process flow diagram (Figure 2) considers a gas source with variable inlet gas conditions ([H₂O], [CO₂], [N₂], and temperature) which is combined with a recycle feed in a mixer. The recycle ratio and flowrate are tested as part of the simulations. The CO₂-rich gas enters a chiller heat exchanger (HEX1) operating across a range of temperatures. A separation column (DRAIN1) is used to simulate a drain in the chiller. The water-depleted gas enters a heater (HEX2) to increase its temperature, which in turn heats the concrete in the reactor. The CO₂ uptake is determined using a calculator function based on the regression model considering the RH, temperature, and [CO₂] conditions. A calculator module was used to calculate the reactor outputs (Section S3 in the Supplementary Information details the reactor model and method used). The regression model is linked to the conversion of the input [Ca(OH)₂] (S12). The predicted mass of CaCO₃ formed in the concrete is recorded in S13 for the model. The CO₂-depleted gas enters another separation column (DRAIN2) where excess water in the reactor is removed (S14), as this simulates drains in the carbonation reactor. The DRAIN2 was maintained at the same temperature as the reactor in the simulation. No extra cooling was applied to that unit. Only excess moisture (where RH >100%) in the reactor would cause condensation. This would occur if the inlet RH was particularly high, enough water was created from the carbonation reaction, and the temperature remained low enough for condensation to occur due to heat loss from the flue gas to the concrete in the reactor. The water flow from DRAIN2 was generally quite minimal and removed <10% of the reactor inlet H₂O due to condensation. The CO₂-depleted gas is released into an

exhaust line which is then emitted from an emissions stack (S10) or input into the recycle line (S11). The flowrate of the recycle line is used to control the recycle ratio (recycle ratio = [flow rate of S11]/[flow rate of S1]) which can act as a dilution of the [CO₂] entering the reactor.

The following scenario was considered for a representative 24-h carbonation period to assess the net CO₂ emissions of the process based on the following unit operation conditions: fixed gas inlet stream (40°C, 14 vol.% CO₂, 7.5 vol.% H₂O, and 78.5 vol.% N₂) and variable operating conditions (10–35°C chiller temperature, 35–70°C heater temperature, and a recycle ratio ranging between 0 and 30, unitless). The gas concentration chosen is representative of natural gas, coal, and biomass emissions streams.^{19,35} To study the influence of the recycle ratio of the process, a reactor inlet flow rate of 1000 kg/h was chosen to ensure sufficient CO₂ was available to completely carbonate the input Ca(OH)₂. To attain a constant reactor inlet flowrate, the gas flowrate was altered between 5 and 1000 kg/h, and the recycle stream was varied between 0 and 995 kg/h where the sum of the two streams equaled 1000 kg/h.

The extent of carbonation (Figure 2; S12) was determined based on the maximum achievable conversion of the OPC, portlandite, and fly ash fractions of the concrete binder. For example, based on the composition of the concrete, its maximum CO₂ uptake is 0.045 g_{CO₂}/g_{solid}. As such, a maximum Ca(OH)₂ content is used to simulate the maximum conversion to calcite:

$$m_{\text{Ca(OH)}_2} = \frac{m_{\text{CO}_2, \text{max}} M_{\text{Ca(OH)}_2}}{M_{\text{CO}_2}}, \quad (6)$$

where $m_{\text{CO}_2, \text{max}}$ is the maximum CO₂ uptake, $m_{\text{Ca(OH)}_2}$ is the Ca(OH)₂ equivalent in the starting mixture, such that the expression additionally includes the molar masses of CO₂ (M_{CO_2}) and Ca(OH)₂ ($M_{\text{Ca(OH)}_2}$). For this concrete formulation, the portlandite content of the concrete was 0.083 g_{CH}/g_{solid} ($m_{\text{Ca(OH)}_2}$). This amount can be scaled to consider any mass of concrete production. For the pilot scale of 10 tonnes per day, the time-averaged portlandite input flowrate into the reactor was 34.54 kg/h. The CO₂ inlet flowrate was much larger than the maximum CO₂ uptake of the solid. Thus, solid conversion (carbonation)

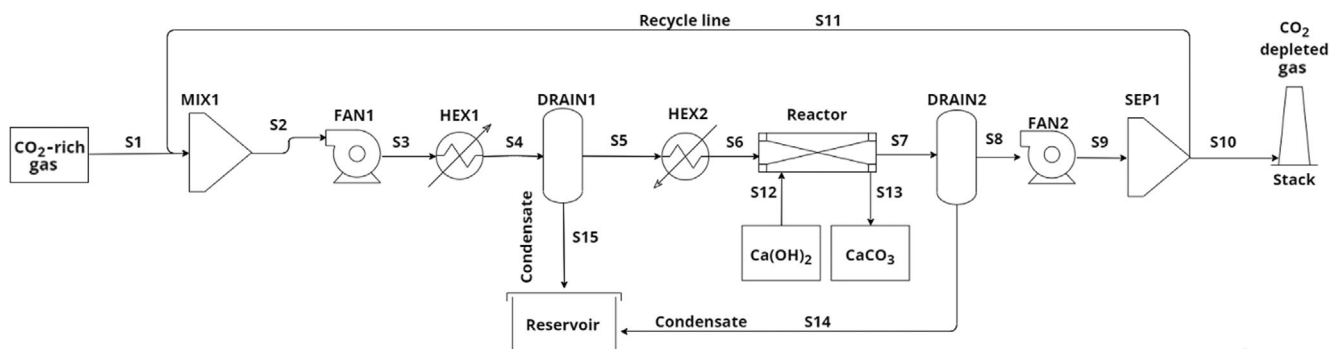


FIGURE 2 The AspenPlus© simulation outline for the concrete carbonation process design.

TABLE 1 The nomenclature and units used in the heat transfer model.

Symbol	Description	Units	Input value
t	Process time	h	12
T	Reactor (outlet) temperature	°C	Output
T_a	Ambient temperature	°C	25
T_{in}	Temperature of inlet stream	°C	35–70
\dot{m}_p	Total inlet molar flow rate	kmol/h	Input
m_b	Mass of concrete blocks	kg	10,000
m_c	Mass of container	kg	3700
C_p	Specific heat capacity of process stream	kJ/kmol °C	Input
C_b	Specific heat capacity of concrete block	kJ/kg °C	0.88 ⁴²
C_c	Specific heat capacity of container	kJ/kg °C	0.47
U	Heat transfer coefficient	kJ/h m ² °C	0.014
A_c	Surface area of container	m ²	128.24 ^a

^aFor a representative pilot plant, a single unit of a carbonation reactor featured the following dimensions: 12.2 m long × 2.4 m wide × 2.6 m high with a wall thickness 0.00195 m.

was not limited due to a lack of CO₂. The regression model used to calculate the extent of conversion of the portlandite applied the following expression:

$$X = a + b \times [\text{CO}_2] - c \times \text{RH} + d \times T, \quad (7)$$

where X is the extent of conversion of $m_{\text{Ca(OH)}_2}$ after 24 h of carbonation, $[\text{CO}_2]$ is the CO₂ concentration within the reactor (vol.%), T is the temperature (°C), and $a, b, c,$ and d are fitting parameters. The carbonation reactor's temperature is controlled by the temperature of the incoming gas that heats the reactor. The following heat transfer model for the static concrete components, reactor, and the incoming gas accounts for this temperature change:

$$\frac{dT}{dt} - \left(\frac{C_p \cdot \dot{m}_p}{C_b \cdot m_b + C_c \cdot m_c} \right) \cdot (T_{in} - T) = - \frac{U \cdot A_c}{C_b \cdot m_b + C_c \cdot m_c} \cdot (T - T_a), \quad (8)$$

where, t is the processing time (h); T is the reactor's outlet temperature (°C); T_a is the ambient temperature (°C); T_{in} is the temperature of the inlet stream (°C); \dot{m}_p is the total inlet molar flow rate of the gas stream (kmol/h); m_b is the mass of CMU in the reactor (kg); m_c is the mass of the carbonation reactor (kg); $C_p, C_b,$ and C_c are the specific heat capacities of the gas stream (kJ/kmol °C), concrete (kJ/kg °C), and container (kJ/kg °C), respectively; U is the heat transfer coefficient (kJ/hm² °C); and A_c is the surface area of the container (m²) (see Table 1). The regression model was developed considering bench-scale reactors that operate at a fixed target temperature; however, in a large-scale reactor, the reactor temperature will steadily increase over time as the reactor inlet gas is used to heat the concrete and the reactor space. To estimate average reactor temperature, Equation (8) was solved to fix the reactor temperature at 12 h (mid-point of the 24-h carbonation cycle). In addition, exothermic reactions from the chemical reactions were not included in the heat transfer equations.

3 | RESULTS AND DISCUSSION

3.1 | Regression model

First, the extent of CO₂ uptake was measured using thermal analysis (see Figure 3A, and Table 2). Thereafter, a regression model was developed to link the extent of CO₂ uptake to the process variables, $[\text{CO}_2]$, T , and RH. This linear model is as described in Equations (7) and (9):

$$X = 0.1660 + 0.0208 \times [\text{CO}_2] - 0.0014 \times \text{RH} + 0.0012 \times T, \quad (9)$$

where, the modeled extent of conversion X_m (conversion, unitless) is the measured CO₂ uptake divided by the theoretical (stoichiometric) CO₂ uptake (4.5 mass % of the total solid mass). Since the RH within the reactor showed fluctuations within ±15%, the average RH over the course of the 24-h carbonation period within the reactor was used as a model input, while the measured temperature (within ±1°C) was specified as is. The ANOVA indicated that the model was significant (p -value = 0.0023) as presented in Table S2. Multivariable quadratic models in each variable were also tested. However, the quadratic models were ill-conditioned and, although predictions for some data points improved, for other data points, the predicted conversions were negative or even above 1.0. Therefore, it was judged that a linear model with a fairly high accuracy was better suited to model the reactor than a quadratic model that can give physically impossible conversions in certain operating ranges.

The model predictions were compared to the experimentally measured extent of conversion (X_e , unitless) as seen in Figure 4B. In general, an acceptable level of agreement between the measured and modeled results was noted ($R^2 = 0.82$, p -value < 0.05; Figure 3B). Three additional model validation conditions (V1, V2, and V3 in Table 2) were used to test the model and compared well with experimental data. Across a wide range of experimental conditions, X_e

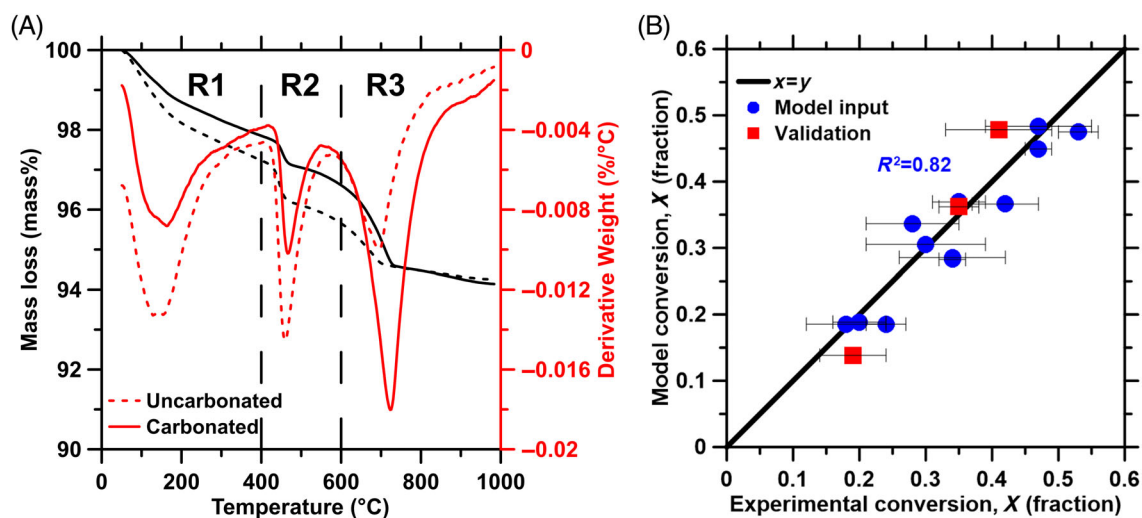


FIGURE 3 (A) Representative thermogravimetric traces of uncarbonated and carbonated concrete samples showing different regions of decomposition: R1: mass loss from cement hydrates, R2: mass loss from portlandite's dehydroxylation, and R3: mass loss from CO₂ evolution, and (B) a comparison of measured (X_e) and modeled (X_m) conversion levels (circles) used for AspenPlus simulation development, and the relevant validation points (squares).

TABLE 2 CO₂ uptake during mineralization across different processing conditions.

Batch ID	[CO ₂] (%)	Measured RH (%)	T (°C)	CO ₂ uptake (fraction of total mass, (±standard deviation))	X_e (fraction) (Standard deviation)	Percentage error (%error)	Absolute error (X_e , %)
1	9	70	43	0.015 (0.004)	0.3 (0.08)	2	0.0068
2	9	55	43	0.018 (0.009)	0.37 (0.06)	-11	0.0422
3	4	48	20	0.009 (0.001)	0.19 (0.02)	8	0.016
4	4	54	65	0.012 (0.002)	0.24 (0.04)	5	0.0116
5	9	23	43	0.017 (0.003)	0.35 (0.07)	6	0.0226
6	14	100	20	0.022 (0.004)	0.44 (0.09)	-22	0.0988
7	14	25	65	0.023 (0.001)	0.47 (0.02)	6	0.0302
8	9	62	11	0.017 (0.002)	0.34 (0.04)	-18	0.0604
9	9	37	74	0.021 (0.001)	0.42 (0.03)	-7	0.0298
10	2	48	43	0.01 (0.002)	0.2 (0.03)	-4	0.008
11	16	57	43	0.026 (0.004)	0.53 (0.08)	-11	0.0594
12	9	86	43	0.017 (0.002)	0.34 (0.05)	-16	0.0556
V1	4	95	20	0.009 (0.001)	0.19 (0.05)	-26	0.0498
V2	8	13.3	40	0.017 (0.003)	0.35 (0.03)	3	0.01178
V3	12	11.3	65	0.019 (0.003)	0.41 (0.08)	17	0.06778

ranged between 0.19 and 0.53 suggesting that the measured extent of CO₂ uptake is sensitive to the process parameters.

The response surfaces shown in Figure 4 show solid conversion at CO₂ concentrations of 4, 9, and 14 vol% for different temperatures and RHs. A higher CO₂ concentration consistently increased the extent of conversion.^{13,14,16} Concrete is a porous solid that allows the transport of aqueous and gaseous species through its interconnected pore network.¹⁶ Within these pores is a solution into which Ca(OH)₂ dissolves and CaCO₃ precipitation occurs. Thus, a higher quantity of pore solution (i.e., a moist concrete), and less connected porosity hinders the transport of CO₂ through the pore spaces. It

should be noted herein that, since carbonation reactions are solution mediated dissolution-precipitation processes, it is desirable to optimize the fraction of pore volume that is air versus water filled since CO₂'s diffusivity through solution is orders of magnitudes smaller than its transport in air (1.6×10^{-13} and 5.19×10^{-7} m²/s, respectively).^{13,36} At the same time, the presence of water is important to promote carbonation reactions. The drying of concrete is enhanced with increasing temperature and reducing RH—which acts to decrease the fraction of water-to-air filled pores (i.e., making the concrete drier).^{17,37,38} Although, the pore (liquid) saturation is reduced with temperature, an increasing temperature also decreases the solubility

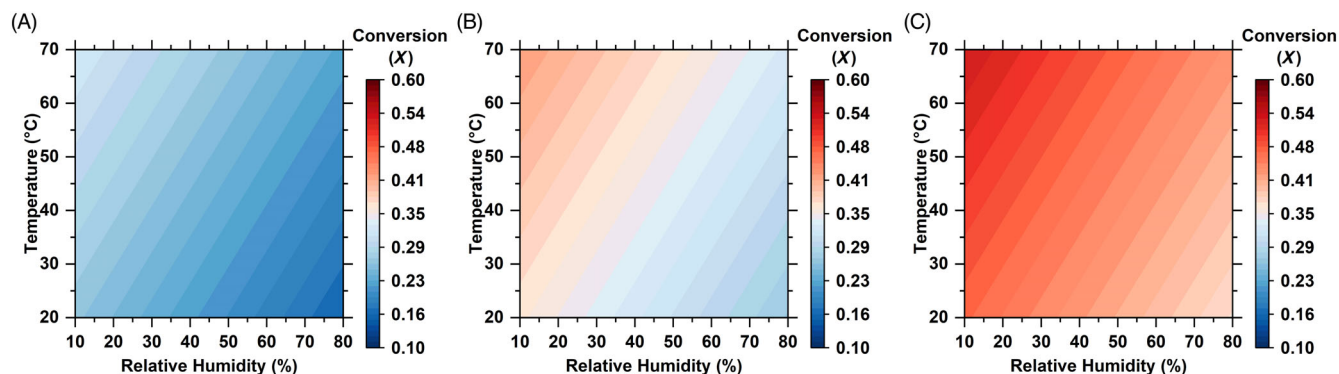


FIGURE 4 The effect of T and RH on the level of conversion X (unitless) at 4, 9, and 14 vol.% CO_2 using the regression model (Equation 9) for solid-phase conversion.

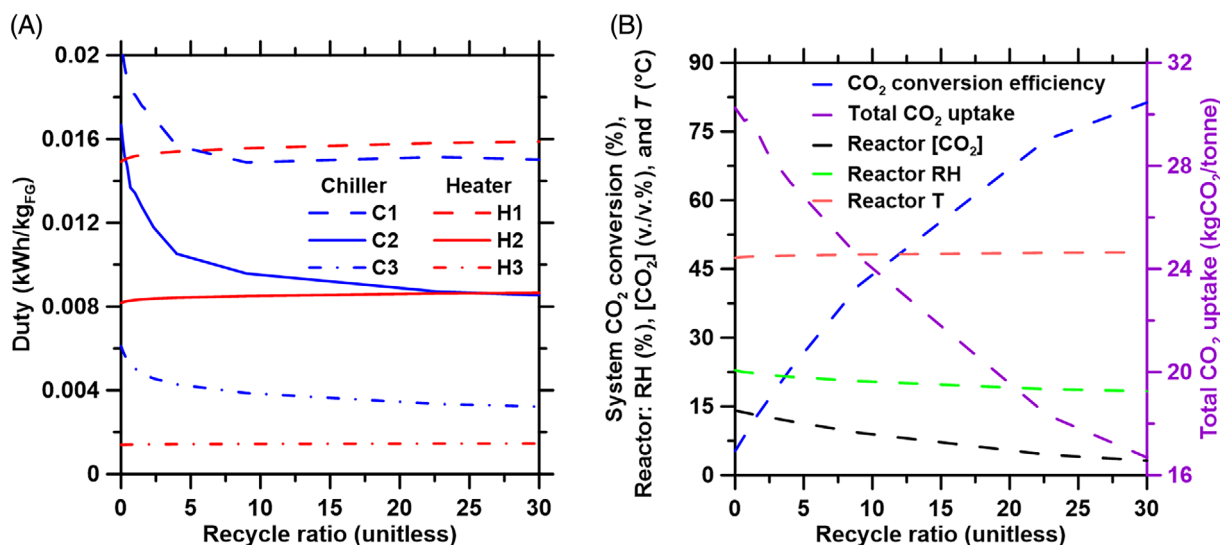


FIGURE 5 (A) Chiller (C) and heater (H) duty requirements across three scenarios: (SC1) chiller 15°C and heater 70°C , (SC2) chiller 20°C and heater 50°C , and (SC3) chiller 30°C and heater 35°C with variable recycle ratio, and (B) the effect of the recycle ratio on conditions inside the reactor, total CO_2 uptake and inlet CO_2 conversion efficiency for Scenario 1 (SC1). For both graphs, the simulated data are for a 24-h carbonation period.

of CO_2 in solution, which could reduce the rate of precipitation of mineral carbonates.¹⁷

3.2 | CO_2 uptake and energy intensity

3.2.1 | Impact of operating conditions

For a fixed inlet gas flowrate, the key process variables are the heater and chiller setpoints and the recycle ratio. To test these variables, a saturated CO_2 source was selected with a composition of 14 vol.% $[\text{CO}_2]$, 7.5 vol.% $[\text{H}_2\text{O}]$, and 78.5 vol.% $[\text{N}_2]$ with an inlet gas temperature of 40°C . A fixed flowrate of gas entered the chiller at 1000 kg/h. To consider the impact of the chiller and heater duties, three scenarios were considered: (SC1) chiller set at 15°C and the heater set at 70°C , (SC2) chiller set at 20°C and heater set at 50°C , and (SC3) chiller

set at 30°C and heater set at 35°C , while in each case the recycle ratio varied. The three scenarios were selected as high, medium, and low energy intensity operating conditions as SC1, SC2 and SC3, respectively. Figure 5A shows how the recycle ratio impacts the cooling and heating duties of the chiller and heater for each scenario. The chiller duty for a recycle ratio of 0 ($RR = 0$) was between $\sim 40\%$ and 90% greater than the minimum value across each recycle ratio as greater quantities of water were condensed at lower recycle ratios when the gas phase is a saturated CO_2 stream, that is, moisture enriched. This contrasts with the $\sim 4\%$ – 6% variation in the heater duty across different recycle ratios. The heater duty remains relatively constant as the composition of the incoming feed does not vary significantly after it exits the chiller, as a result of which the heat capacity of the gas is effectively unchanged. The slight increase observed was attributed to the slightly increased mass flowrate after the chiller, as less water was removed after the chiller at higher recycle ratios. These trends were

observed for SC1–SC3 and were offset by the change in temperature across the heat exchanger.

Figure 5B shows that the recycle ratio has a significant impact on CO₂ uptake and the extent of gaseous CO₂ conversion efficiency across the system for SC1. The CO₂ conversion efficiency was calculated as:

$$\text{CO}_2 \text{ conversion (\%)} = \left(1 - \frac{m_{\text{CO}_2, \text{S1}} - m_{\text{CO}_2, \text{S10}}}{m_{\text{CO}_2, \text{S1}}}\right) \times 100, \quad (10)$$

where $m_{\text{CO}_2, \text{S10}}$ is the mass flowrate of CO₂ in stream 10 (kg/h), and $m_{\text{CO}_2, \text{S1}}$ is the mass flowrate of CO₂ in Stream 1 (kg/h) as shown in Figure 2. The RH, temperature, and [CO₂] varied to different extents with the recycle ratio. The [CO₂] concentration decreased as the recycle ratio increased causing a reduction in the total amount of CO₂ converted to CaCO₃ as the concentration of CO₂ in the reactor diminished. A lower reactor RH was observed with an increasing recycle ratio which, although favorable for CO₂ uptake, was counterbalanced by the impact of the CO₂-diluted feed entering the reactor. At a fixed inlet temperature, the total CO₂ uptake was highest at low recycle ratios; although, expectedly, the lowest CO₂ conversion efficiency was observed for the single pass case (recycle ratio of zero). The extent of conversion increased to 81% at a recycle ratio of 30. In other words, depending on the size of the concrete plant and the CO₂ source that is being utilized, the recycle ratio may be an influential parameter in determining whether the process should be operated as a single pass (RR = 0) or multipass (RR > 0) configuration. That said, a minimum gas flowrate entering the carbonation reactor is required to ensure uniform gas distribution across the surface of the concrete. Therefore, if a low flow rate CO₂ source is used, a high(er) recycle ratio may be necessary to maintain a uniform surface coverage of the gas across the concrete surface through the reactor.¹² For these conditions, the CO₂ utilization efficiency (i.e., the amount of CO₂ utilized as a function of the amount of CO₂ input into the system) will increase but total uptake could, in fact, decrease over short carbonation periods (<24 h carbonation time).

3.2.2 | Net CO₂ emissions and system optimization

The net CO₂ emissions resulting from the carbonation process are dictated by the extent of CO₂ uptake and the CO₂ emissions associated with gas processing (i.e., electricity use, see Supplementary Information Section S4). Considering electricity as the energy input for production, the grid emissions factor (eGrid) is important to consider (i.e., kgCO₂ emitted per kWh of electricity produced). This factor differs across energy sources: renewables: 0–0.18 kgCO₂/kWh, natural gas: 0.41 kgCO₂/kWh, oil: 0.81 kgCO₂/kWh, and coal: 0.98 kWh/kgCO₂ according to current US Environmental Protection Agency data.³⁹ Depending on the location or waste heat recovery, the net CO₂ emissions vary as follows:

$$N_{\text{CO}_2} = E \cdot \text{eGrid} - m_{\text{CO}_2, \text{T}}, \quad (11)$$

where, N_{CO_2} is net CO₂ emissions (kgCO₂), E is the total (the sum of the duties of the fans, chiller, and heater) electrical energy required by the system (kWh), eGrid is the grid emissions factor (kgCO₂/kWh), and $m_{\text{CO}_2, \text{T}}$ is the amount of CO₂ taken up into the concrete (kgCO₂). The duty of the chiller was used to determine the refrigeration energy required to reduce the flue gas temperature to target values. The total energy, E , was calculated for a 24-h carbonation period and the indirect CO₂ emissions was calculated by the eGrid value (kgCO₂/kWh).

A negative N_{CO_2} indicates more CO₂ has been removed during carbonation than was required for production. Figure 6A–C shows the energy intensity of the process as a function of chiller and heater conditions per unit mass of CO₂ uptake at recycle ratios of 2, 10, and 30, respectively. This analysis estimated energy efficiencies of air-cooled chiller and electrical heaters as 80% and 95%, respectively. The data suggest that a low recycle ratio is the least energy intensive means to maximize CO₂ uptake on account of maintaining higher levels of [CO₂] within the reactor and thus ensuring greater CO₂ uptake into the solid phase (Figure 6A). The [CO₂] levels for the different recycle ratios (14 < RR2 < 14.1 vol.% CO₂, 10 < RR10 < 11 vol.% CO₂, and 2 < RR30 < 3 vol.% CO₂) greatly impact CO₂ uptake. Although increasing the recycle ratio reduces the RH as less water is introduced from the gas, the higher CO₂ concentration that exists at lower RRs is far more influential than maintaining a low RH. Using the US average grid emissions factor of 0.37 kgCO₂/kWh,³⁹ it is possible to determine the net CO₂ impact of the process as shown in Figure 6D–F. The negative values indicate (net) CO₂ removal.

In spite of the energy requirements of gas processing, it is noted that maintaining a low(er) heater and high(er) chiller temperature result in negative net CO₂ emissions at low recycle ratios. Obviously, if renewable energy is used to power the carbonation process, the grid emissions are effectively irrelevant in terms of affecting the net CO₂ footprint of the process. In this case, more energy intensive processing can be applied to further enhance the CO₂ uptake (see Figure 7A). The AspenPlus© optimization module was used to analyze varying eGrid values to determine the net CO₂ emissions (emissions, or removal) using Equation (11) as the cost function. This analysis shows that, for decarbonized grids, the representative formulation used herein can achieve a net removal of ~28 kgCO₂ uptake/tonne of concrete. This level of CO₂ uptake corresponds to an energy intensity of 5.9 kWh/kgCO₂. On the other hand, for the average US grid (eGrid ~0.37 kgCO₂/kWh), the net energy intensity of the process has to be lower than 2.67 kWh/kgCO₂ to produce a carbon negative concrete (see Figure 7B). Expectedly, a considerable reduction in the energy intensity of the process can be achieved if waste heat were available, for example, at an industrial CO₂ source, but this requires co-location of concrete production at a CO₂ emissions/industrial site—an atypical circumstance.

For comparison of the embodied carbon intensity of the carbonated concrete studied herein and a traditional OPC-based binder

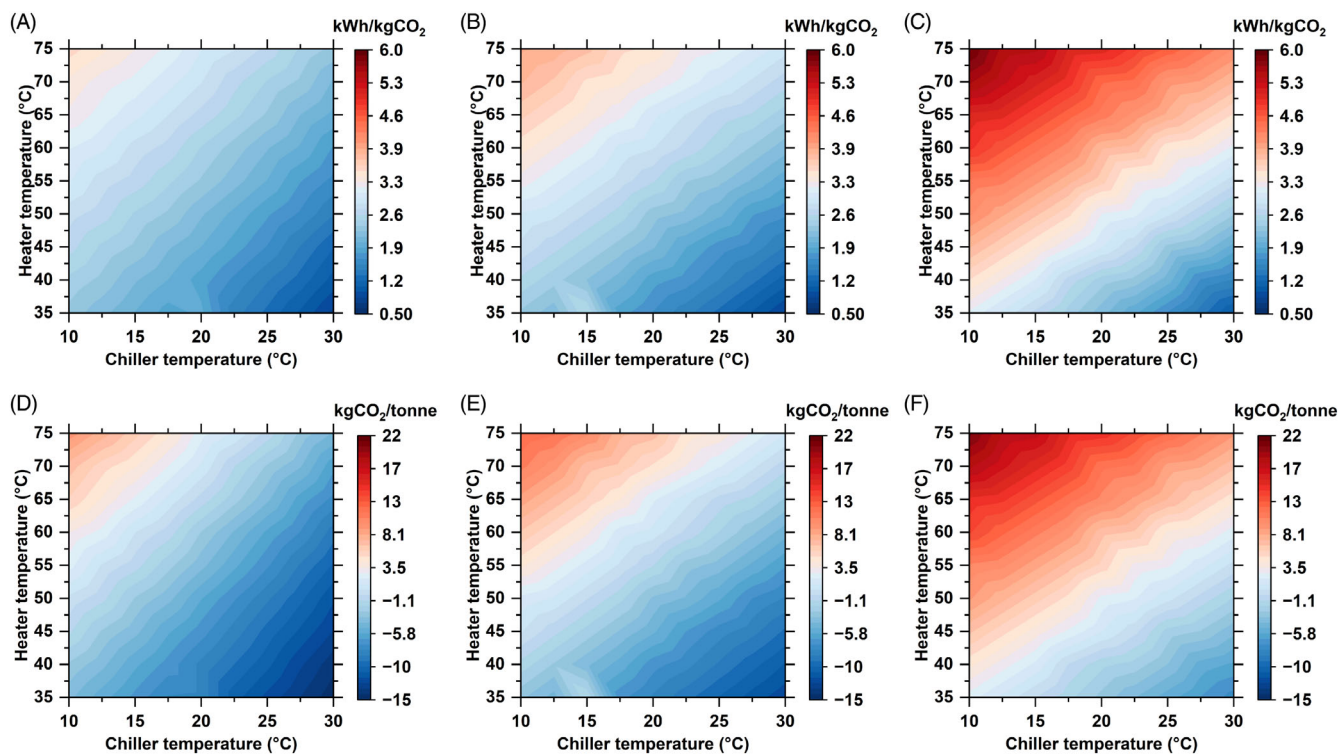


FIGURE 6 The energy intensity of the carbonation process for different chiller and heater set-points for recycle ratios (RRs) f : (A) 2, (B) 10, and (C) 30. The net CO₂ emissions of the process for the US average grid considering an eGrid value of 0.37 kgCO₂/kWh for recycle ratios of (D) 2, (E) 10, and (F) 30.

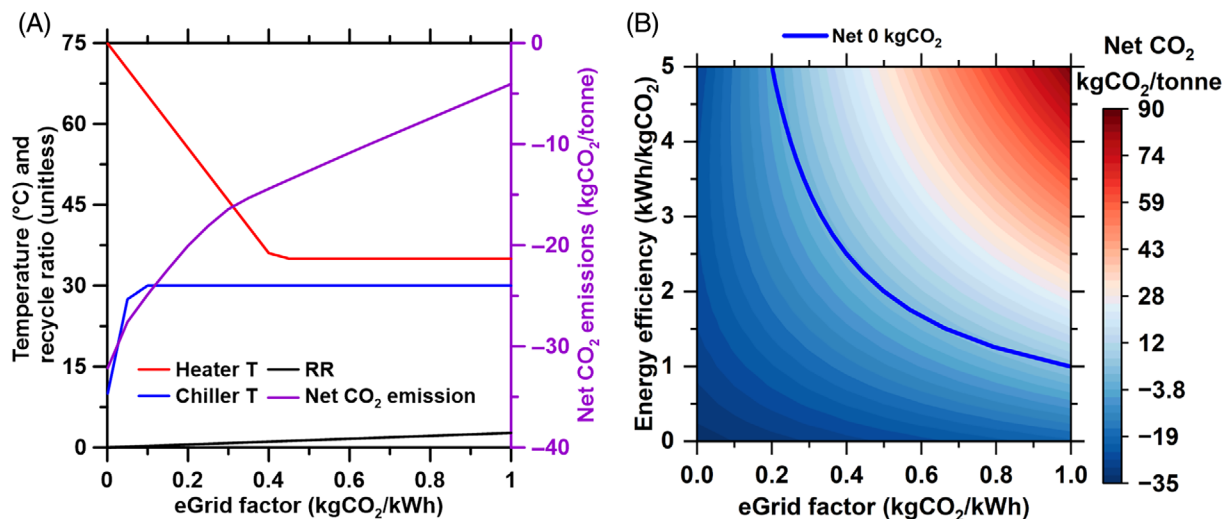


FIGURE 7 (A) The minimum net CO₂ emissions of the carbonation process following 24 h of processing for different heater and chiller set-points and recycle ratios, and (B) the net CO₂ emissions of carbonation across the range of operating conditions as a function of the process's energy intensity and eGrid value of input electricity.

system, the specific mixture formulation and the carbonation steps can be compared against a traditional concrete system. The embodied carbon intensity of the raw materials are: OPC, 0.928 kgCO₂/kg⁴⁰; portlandite, 0.768 kgCO₂/kg⁴⁰; fly ash, 0 kgCO₂/kg; coarse aggregate, 0.00142 kgCO₂/kg⁴¹; and fine aggregate, 0.00091 kgCO₂/kg.⁴¹ The fly ash is considered to contribute 0 kgCO₂/kg as it is considered a

byproduct from another process. On a material-only basis, a 20 mass % OPC system using the same aggregate gradation yields 186.4 kgCO₂/tonne of concrete and the formulation used herein produces 132 kgCO₂/tonne. The net CO₂ uptake from the carbonation step further can reduce the embodied carbon intensity by up to 28 kgCO₂ (i.e., thereby reducing the embodied carbon intensity to 104 kgCO₂/

tonne). Considering a net CO₂ reduction from 0 to 28 kgCO₂/tonne, the embodied carbon intensity (eCI) reduction produced via accelerated carbonation can thus range from ~30% to 45%. And, prominently pre-commercial operational trials of CarbonBuilt™'s CMU have shown eCI reductions up to 70%.

4 | SUMMARY AND CONCLUSIONS

An AspenPlus© model of an accelerated concrete carbonation process utilizing a water saturated CO₂-rich gas source was developed. A regression model was used to estimate the extent of Ca(OH)₂ to CaCO₃ for the following operating conditions within the reactor: 15 < T < 65°C, 10 < RH < 80%, and 4 < [CO₂] < 14 vol.%. The regression model identified that the [CO₂] was a dominant factor that affected solid-phase conversion. Across the reactor conditions studied, a conversion of ~20–55 mass % of the Ca(OH)₂ was measured. A fixed gas inlet stream (e.g., 14 vol.% [CO₂], 7.5 vol.% [H₂O], and 78.5 vol.% [H₂O] with a temperature of 40°C) was used to assess the effects of operating conditions on the CO₂ uptake, CO₂ conversion efficiency, and net CO₂ emissions. The process simulations identified that a single pass carbonation process (RR = 0), low chiller (15°C) and high heater (70°C) temperatures are ideal to maximize CO₂ uptake. The limitations of these process conditions are its high energy intensity and low CO₂ gas conversion. To achieve higher CO₂ gas conversions, a larger recycle ratio is required to achieve gas conversions of greater than 80 mass %. The optimum operating conditions for minimizing net CO₂ emissions considering the chiller and heater temperatures, and recycle ratio are dictated by the eGrid factor. At low eGrid factors (eGrid < 0.2 kgCO₂/kWh) the energy intensity of the process can be as high as 5.9 kWh/kgCO₂ to achieve net negative CO₂ emissions, that is, to achieve net CO₂ uptake as high as 28 kgCO₂/tonne of concrete. The net CO₂ emissions reduction potential decreases as the eGrid factor increases. Across a broad range of eGrid factors, and for the formulation examined herein, accelerated carbonation can reduce the eCI of a CMU-type masonry formulation by 30%–45%. Expectedly, enhancing OPC replacement with other waste productions would result in additional eCI reductions. This modeling approach developed herein informs process design and operations so as to optimize an accelerated carbonation process to: (a) minimize energy intensity, (b) maximize CO₂ uptake and eCI reductions, and (c) to identify optimal mixture formulations that allow realization of desirable cost, CO₂ and (materials-based) eCI metrics.

AUTHOR CONTRIBUTIONS

Dale P. Prentice: Formal analysis (lead); investigation (lead); methodology (lead); project administration (lead); software (lead); supervision (lead); visualization (lead); writing – original draft (lead); writing – review and editing (lead). **Othman AlShareedah:** Investigation (supporting); methodology (supporting); validation (supporting). **Manas Sarkar:** Investigation (supporting); methodology (supporting); validation (supporting). **Jenny Arabit:** Investigation (supporting); writing – original draft (supporting). **Iman Mehdipour:**

Conceptualization (supporting); methodology (supporting). **Shaik Afzal:** Investigation (supporting); methodology (supporting); software (supporting). **Junwei Luo:** Investigation (supporting); software (supporting). **Fahim Abdullah:** Software (supporting); writing – review and editing (supporting). **Sungil Yun:** Methodology (supporting); software (supporting). **Panagiotis D. Christofides:** Methodology (equal); supervision (equal); writing – review and editing (equal). **Dante Simonetti:** Supervision (equal); writing – review and editing (equal). **Gaurav Sant:** Conceptualization (equal); funding acquisition (equal); project administration (equal); visualization (equal); writing – review and editing (equal).

ACKNOWLEDGMENTS

This research was conducted in the Laboratory for the Chemistry of Construction Materials (LC²) at UCLA. The authors gratefully acknowledge the support provided by these laboratories. The contents of this paper reflect the views and opinions of the authors, who are responsible for the accuracy of the datasets presented herein, and do not reflect the views and/or policies of the funding agencies, nor do the contents constitute a specification, standard or regulation.

FUNDING INFORMATION

The authors acknowledge financial support for this research from the Department of Energy: Office of Fossil Energy via the National Energy Technology Laboratory (NETL; DE-FE0031915), the University of California's Office of the President via the Carbon Neutrality Initiative (UCOP-CNI), and the Pritzker Chair in Sustainability.

DATA AVAILABILITY STATEMENT

Regression model data for Equation 7 was collected in triplicate for determining the fitting values from the data, this is reflected in the standard deviation values in Table 2 and the error bars shown in Figure 3B. The experimental matrix for development of the design of experiments is submitted in Section S1 of the supplementary information. The modeling results for Figures 4–7 are included in the excel file submitted as supplementary information labeled “Data availability and reproducibility.xlsx.” The Aspen simulation file is not submitted as supplementary information for confidentiality considerations. These data were generated from Aspen simulations following the procedure described in “Section Heat and mass transfer modeling using AspenPlus©.” The data and modeling results for Section S2 concerning the isothermal calorimetry and thermodynamic modeling results are included in the excel file submitted as supplementary information labeled “Data availability and reproducibility.xlsx.” Experimental data were generated as part of the current study, and thermodynamic modeling was conducted using GEMSelektor v3.6. The modeling results used to plot the data for Section “S4: Gas processing” are included in the excel file submitted as supplementary information labeled “Data availability and reproducibility.xlsx.” These data were generated from Aspen simulations following the procedure described in “Section Heat and mass transfer modeling using AspenPlus©.” All tabs in the excel file “Data availability and reproducibility.xlsx” are labeled with the accompanying figure number.

ORCID

Dale P. Prentice  <https://orcid.org/0000-0002-4980-8751>

Panagiotis D. Christofides  <https://orcid.org/0000-0002-8772-4348>

Dante Simonetti  <https://orcid.org/0000-0002-5708-460X>

REFERENCES

- Andrew R. Global CO₂ emissions from cement production. *Earth Syst Sci Data Discuss.* 2018;10:195-217. doi:10.5281/ZENODO.831455
- Taylor HFW. *Cement Chemistry*. Thomas Telford; 1997.
- Mehta PK, Monteiro PJ. *Concrete: Microstructure, Properties, and Materials*. 3rd ed. McGraw-Hill Education; 2014.
- Gartner EM, Macphee DE. A physico-chemical basis for novel cementitious binders. *Cem Concr Res.* 2011;41(7):736-749. doi:10.1016/j.cemconres.2011.03.006
- Miller SA, Horvath A, Monteiro PJM. Readily implementable techniques can cut annual CO₂ emissions from the production of concrete by over 20%. *Environ Res Lett.* 2016;11(7):074029. doi:10.1088/1748-9326/11/7/074029
- Mehdipour I, Falzone G, La Plante EC, Simonetti D, Neithalath N, Sant G. How microstructure and pore moisture affect strength gain in portlandite-enriched composites that mineralize CO₂. *ACS Sustain Chem Eng.* 2019;7(15):13053-13061. doi:10.1021/acssuschemeng.9b02163
- Rostami V, Shao Y, Boyd AJ, He Z. Microstructure of cement paste subject to early carbonation curing. *Cem Concr Res.* 2012;42(1):186-193. doi:10.1016/j.cemconres.2011.09.010
- Ghafari E, Costa H, Júlio E. Statistical mixture design approach for eco-efficient UHPC. *Cem Concr Compos.* 2015;55:17-25. doi:10.1016/j.cemconcomp.2014.07.016
- ASTM. C140/C140M-21 *Test Methods for Sampling and Testing Concrete Masonry Units and Related Units*. ASTM International; 2021. doi:10.1520/C0140_C0140M-21
- Huang TY, Chiueh PT, Lo SL. Life-cycle environmental and cost impacts of reusing fly ash. *Resour Conserv Recycl.* 2017;123:255-260. doi:10.1016/j.resconrec.2016.07.001
- Lothenbach B, Kulik DA, Matschei T, et al. Cemdata18: a chemical thermodynamic database for hydrated Portland cements and alkali-activated materials. *Cem Concr Res.* 2019;115:472-506. doi:10.1016/j.cemconres.2018.04.018
- Mehdipour I, Falzone G, Prentice D, Neithalath N, Simonetti D, Sant G. The role of gas flow distributions on CO₂ mineralization within monolithic cemented composites: coupled CFD-factorial design approach. *React Chem Eng.* 2021;6(3):494-504. doi:10.1039/D0RE00433B
- Kashef-Haghighi S, Shao Y, Ghoshal S. Mathematical modeling of CO₂ uptake by concrete during accelerated carbonation curing. *Cem Concr Res.* 2015;67:1-10. doi:10.1016/j.cemconres.2014.07.020
- Papadakis VG, Vayenas CG, Fardis MN. A reaction engineering approach to the problem of concrete carbonation. *AIChE J.* 1989; 35(10):1639-1650. doi:10.1002/aic.690351008
- Jang JG, Lee HK. Microstructural densification and CO₂ uptake promoted by the carbonation curing of belite-rich Portland cement. *Cem Concr Res.* 2016;82:50-57. doi:10.1016/j.cemconres.2016.01.001
- Thiery M, Villain G, Dangla P, Platret G. Investigation of the carbonation front shape on cementitious materials: effects of the chemical kinetics. *Cem Concr Res.* 2007;37(7):1047-1058. doi:10.1016/j.cemconres.2007.04.002
- Zhang D, Ghoulah Z, Shao Y. Review on carbonation curing of cement-based materials. *J CO₂ Util.* 2017;21:119-131. doi:10.1016/j.jcou.2017.07.003
- García-González CA, el Grouh N, Hidalgo A, et al. New insights on the use of supercritical carbon dioxide for the accelerated carbonation of cement pastes. *J Supercrit Fluids.* 2008;43(3):500-509. doi:10.1016/j.supflu.2007.07.018
- Amann JMG, Bouallou C. CO₂ capture from power stations running with natural gas (NGCC) and pulverized coal (PC): assessment of a new chemical solvent based on aqueous solutions of N-methyldiethanolamine + triethylene tetramine. *Energy Procedia.* 2009;1(1):909-916. doi:10.1016/j.egypro.2009.01.121
- You X, Hu X, He P, Liu J, Shi C. A review on the modelling of carbonation of hardened and fresh cement-based materials. *Cem Concr Compos.* 2022;125:104315. doi:10.1016/j.cemconcomp.2021.104315
- Prentice DP, Raab S, Sant GN. *Field Demonstration of the ReversaTM Mineral Carbonation Process Using Coal and Natural Gas Flue Gas Streams at the National Carbon Capture Center*; 2021.
- National Academies of Sciences. *Gaseous Carbon Waste Streams Utilization: Status and Research Needs*. The National Academies Press; 2018. doi:10.17226/25232
- Song C, Pan W, Srimat ST, et al. Tri-reforming of methane over Ni catalysts for CO₂ conversion to syngas with desired H₂/CO ratios using flue gas of power plants without CO₂ separation. *Studies in Surface Science and Catalysis*. Vol 153. Elsevier; 2004:315-322. doi:10.1016/S0167-2991(04)80270-2
- Drage TC, Snape CE, Stevens LA, et al. Materials challenges for the development of solid sorbents for post-combustion carbon capture. *J Mater Chem.* 2012;22(7):2815-2823. doi:10.1039/C2JM12592G
- Wang X, Song C. Carbon capture from flue gas and the atmosphere: a perspective. *Front Energy Res.* 2020;8:560849. doi:10.3389/ferg.2020.560849
- Pantaleo AM, Fordham J, Oyewunmi OA, Markides CN. Intermittent waste heat recovery: investment profitability of ORC cogeneration for batch, gas-fired coffee roasting. *Energy Procedia.* 2017;129:575-582. doi:10.1016/j.egypro.2017.09.209
- Lasek JA, Kopczyński M, Janusz M, Iluk A, Zuwała J. Combustion properties of torrefied biomass obtained from flue gas-enhanced reactor. *Energy.* 2017;119:362-368. doi:10.1016/j.energy.2016.12.079
- ASTM C33. *Standard Specification for Concrete Aggregates*. ASTM International; 2018. Accessed May 9, 2022. https://www.astm.org/c0033_c0033m-18.html
- Maheswaran S, Ramachandra Murthy A, Ramesh Kumar V, Karunanithi A. Characterisation studies on the particle size effect of calcium carbonate in high-strength concrete. *Mag Concr Res.* 2021; 73(13):661-673. doi:10.1680/jmacr.19.00375
- Vogler N, Drabetzki P, Lindemann M, Kühne HC. Description of the concrete carbonation process with adjusted depth-resolved thermogravimetric analysis. *J Therm Anal Calorim.* 2022;147(11):6167-6180. doi:10.1007/s10973-021-10966-1
- Stat-Ease, Inc. *Design-Expert 7.0 User's Guide*. 2005.
- Hanson K. A closer look: accelerated curing. *Natl Precast Concr Assoc.* 2016;Q1:9-12.
- Falzone G, Mehdipour I, Neithalath N, Bauchy M, Simonetti D, Sant G. New insights into the mechanisms of carbon dioxide mineralization by portlandite. *AIChE J.* 2021;67(5):e17160. doi:10.1002/aic.17160
- Chen CC, Song Y. Generalized electrolyte-NRTL model for mixed-solvent electrolyte systems. *AIChE J.* 2004;50(8):1928-1941. doi:10.1002/aic.10151
- US EPA. Sources of greenhouse gas emissions. 2015. Accessed June 9, 2022 <https://www.epa.gov/ghgemissions/sources-greenhouse-gas-emissions>
- Pinsent BRW, Pearson L, Roughton FJW. The kinetics of combination of carbon dioxide with hydroxide ions. *Trans Faraday Soc.* 1956;52: 1512. doi:10.1039/tf9565201512
- Wirtanen L, Penttala V. Influence of temperature and relative humidity on the drying of concrete. *Concr Sci Eng.* 2000;2:39-47.
- Younsi A, Bordy A, Aggoun S, Fiorio B. Hydration-drying interactions in OPC pastes blended with recycled OPC paste fine powder: critical

- curing relative humidity hampering hydration. *Construct Build Mater.* 2018;190:403-413. doi:[10.1016/j.conbuildmat.2018.09.132](https://doi.org/10.1016/j.conbuildmat.2018.09.132)
39. US Environmental Protection Agency (EPA). *Emissions & Generation Resource Integrated Database (eGRID)*, 2020. Office of Atmospheric Programs, Clean Air Markets Division; 2022:5. <https://www.epa.gov/egrid>.
 40. National Renewable Energy Laboratory. *U.S. Life Cycle Inventory Database*. 2012.
 41. Marceau M, Nisbet M, VanGeem M. *Life Cycle Inventory of Portland Cement Concrete*. Portland Cement Association; 2006.
 42. NCMA. *NCMA TEK-6-16A: Heat Capacity (HC)*. Values for Concrete Masonry Walls; 2008.

SUPPORTING INFORMATION

Additional supporting information can be found online in the Supporting Information section at the end of this article.

How to cite this article: Prentice DP, AlShareedah O, Sarkar M, et al. Process modeling guides operational variables that affect CO₂ utilization during the accelerated carbonation of concrete. *AIChE J.* 2024;70(5):e18387. doi:[10.1002/aic.18387](https://doi.org/10.1002/aic.18387)